# RELATIVE POSITION SENSING AND AUTOMATIC CONTROL FOR OBSERVATION IN THE MIDWATER BY AN UNDERWATER VEHICLE

**Aaron M. Plotnik and Stephen M. Rock**
{aplotnik, rock}@stanford.edu

Aerospace Robotics Laboratory, Stanford University
Durand Bldg Room 028, 496 Lomita Mall, Stanford, CA 94305-4035
and
Monterey Bay Aquarium Research Institute
7700 Sandholdt Road, Moss Landing, CA 95039-9644

## ABSTRACT

A vision-based automatic tracking and observation system installed on an ROV has successfully tracked midwater ocean animals (such as jellyfish) in Monterey Bay, California. This system uses stereo vision to localize the tracking vehicle with respect to the target of interest and closes control loops to maintain the target in the views of the cameras. The vision and control algorithms have been reported previously. This paper documents the partial redesign of the system in response to issues identified during extensive field testing of the system. The sensing system has been redesigned with the specific objectives of improving initialization, achieving better robustness to disturbances, and enabling tracking of smaller specimens. All of these improvements are achieved by redesigning the stereo camera system to increase significantly the volume that is viewable by both cameras. Also, an optional heading control loop now augments the control architecture to prevent sustained clocking of the vehicle due to disturbances in the tracking control system's null space. With these design improvements, the automatic tracking and observation system has been fielded as a pilot aid on the ROV *Ventana*, and has proven capable of tracking specimens that vary widely in size, appearance and behavior.

## 1 INTRODUCTION

A sensing and control system that enables autonomous tracking of animals in the midwater by ROVs (and potentially by AUVs) has been developed, demonstrated and deployed on the ROV *Ventana* as a pilot aid. The basic vision and control algorithms as well as preliminary field test results using this system have been reported previously [1-3]. This paper presents new results from the continued development and testing of the system. Issues encountered during extensive field testing are presented, along with the design changes made to overcome or mitigate these issues. Results presented in this paper document the system's performance from more recent field tests of the ROV pilot aid and demonstrate the improved system's viability in tracking a range of observation specimens that vary widely in size, appearance and motion behavior.

Human-piloted ROVs have enabled biologists to observe individual animals in the ocean and collect data about their behavior in their natural habitat [4-7]. Tracking an animal for long durations is fatiguing for a pilot, however. Hence, an automated capability offers the potential for greatly extending the periods over

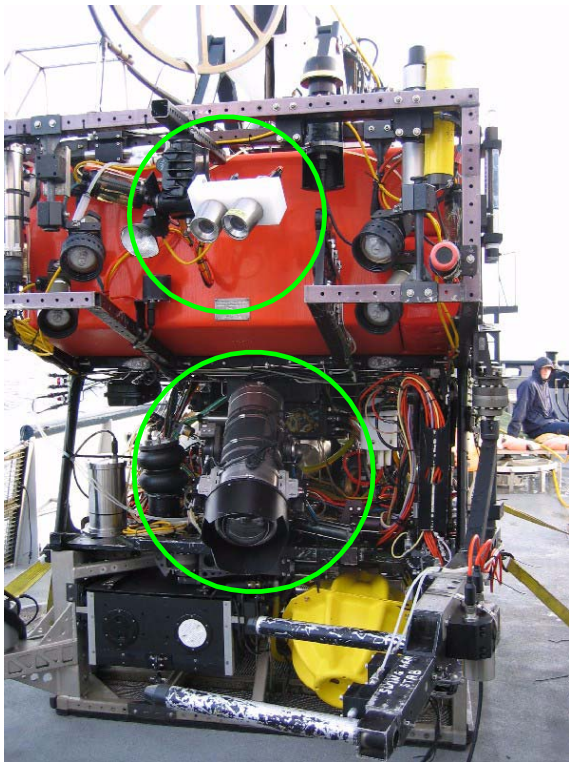

**Figure 1** The ROV *Ventana*, configured with cameras for midwater tracking (circled, top center). The high definition science camera is indicated in the lower circle.

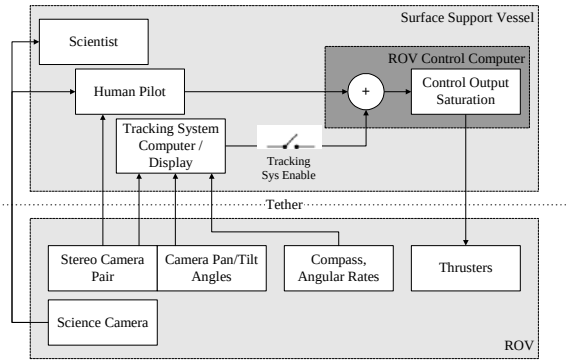


**Figure 2** Block diagram of tracking system hardware and its interactions with the human ROV pilot and scientist.

which an animal can be observed. The automated tracking system presented here uses a stereo camera system (a photograph is included in Figure 1) to measure relative position to the specimen of interest and closes control loops using the vehicle's thrusters to maintain the specimen in view of the cameras. The system architecture is shown in Figure 2. The control objectives are represented in a cylindrical coordinate system that maps measured relative position to standoff distance, relative heading and relative altitude to the target, as illustrated in Figure 3.

Extensive field testing has exposed several issues with the initial configuration of this system. These include limitations on the minimum size of the tracked specimen, difficulties in initialization of the system by the ROV pilot, and common occurrences of sustained clocking of the vehicle around the specimen. In response to these issues, the system has been partially redesigned and augmented to improve operability and robustness and to expand the range of animals that can be tracked (the system was until recently limited to targets that could be seen at a standoff distance of about 1 meter or more).

The stereo camera system has been redesigned to increase the volume viewable by both control cameras substantially. The tracking system depends on an uninterrupted ability to sense relative position to the specimen. To maintain this continuity, the specimen must be kept in the common viewing volume at all times. Hence, the size and geometry of this volume impart constraints upon the accuracy of the automatic control system (and of the ROV pilot when initializing). Since easing these constraints, the system is significantly easier for the ROV pilot to initialize and the operational envelope is expanded to smaller targets that are only visible at standoff distances of 0.5 meters or less.

To resolve the vehicle clocking issue, an optional low-bandwidth heading loop now augments the tracking control loops to stabilize heading of the vehicle while tracking a target. This secondary control loop corrects for the unmodeled thruster mapping errors and disturbances that induce the clocking via simultaneous yawing and lateral motions.

A wide variety of specimens have been tracked by the system, including 89 minutes of uninterrupted tracking of a *Ptychogena* jellyfish between 5-10 centimeters in diameter, several examples of tracking large jellyfish such as *Solmissus*, and tracking of small squid such as *Gonatus*. Since the redesign, recent field trials have demonstrated the system's ability to track smaller and more agile targets such as a larval flatfish traveling at over 7 centimeters per second and the jellyfish *Aegina*, which are on the order of 2

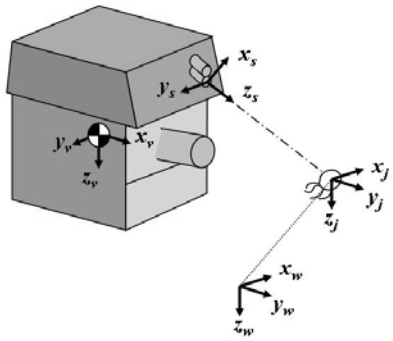


(a)

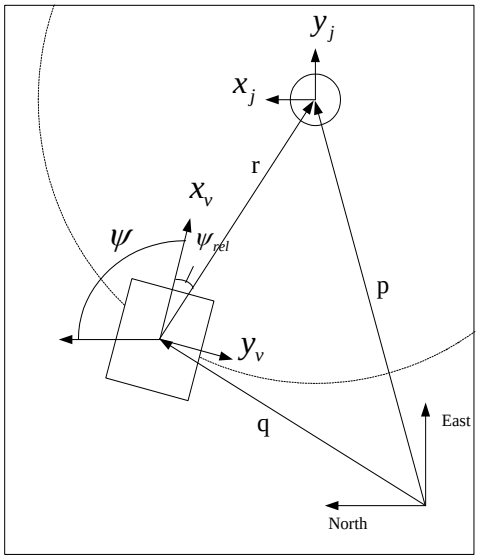


(b)

**Figure 3** Vision-based sensing (a) coupled with cylindrical control system (b) for tracking of midwater ocean animals. In (a), subscripts indicate frames as water (w), sensor (s), vehicle (v) and jelly (j). In (b), the vehicle is indicated by the rectangle, the target jelly by the circle.

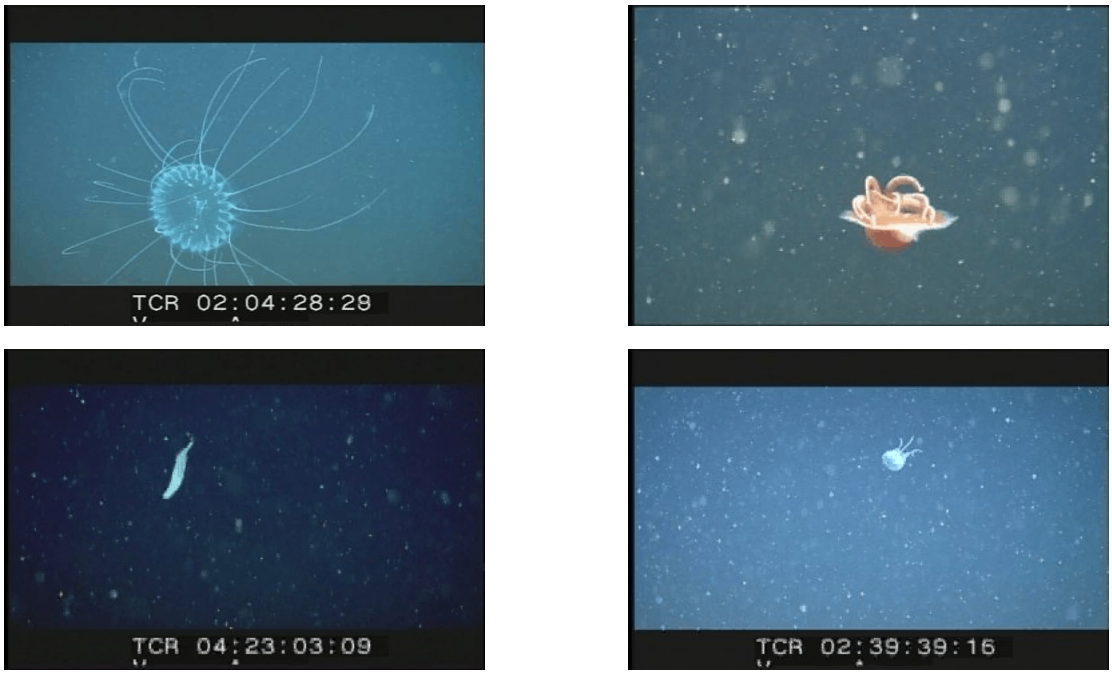


**Figure 4** Example photographs of tracked animals taken by the automatic tracking system. The first row are samples tracked before the design improvements documented by this paper, the second row includes examples that were only enabled after these redesigns. Top left: *Solmissus* (large medusa jellyfish), top right: *Gonatus* (a small squid), bottom left: a larval flatfish, bottom right: *Aegina* (a very small medusa jellyfish).

centimeters in diameter.

The remainder of this paper is structured as follows: Section 2 provides a brief overview of the tracking system. Section 3 discusses the difficulties with initialization and disturbance tolerance that have been observed during field testing and presents an analysis of the camera sensor in terms of the constraints it imposes on the performance of the control system. A redesigned camera system is presented based on this analysis. Section 4 addresses the issues with sustained clocking about the target and documents a new heading hold loop that has the effect of locking the cylindrical control system onto a fixed point on the circumference of the circle. Finally, Section 5 presents tracking results using the updated system.

## 2 SYSTEM OVERVIEW

The vision-based automatic tracking system has been demonstrated as a pilot assist on the ROV *Ventana* in Monterey Bay, CA [1-3]. The close-up photographs of Figure 4 were taken during recent experiments using this system. The system's architecture, including interfaces to the human operator(s), is depicted in Figure 2.

The tracking system is operated from a surface support vessel, the R/V *Point Lobos*. The ROV is operated by a human pilot who is directed by a scientist to choose a specimen in the midwater to track. To initialize the system, the ROV pilot positions the vehicle such that the specimen is visible in the viewing cones of both control cameras, and at a close enough range that the vision algorithms on the tracking system computer can "see" the specimen. With the animal visible in both cameras, the tracking system uses the calibrated intrinsic parameters of each camera and the calibrated parameters of the stereo rig to triangulate to the animal. Thus, a relative position for use by the automatic control system is generated. When satisfied that the system is tracking correctly and the vehicle's relative position to the target is steady, the automatic control system is engaged.

The coordinate frames used by the tracking system are illustrated in Figure 3. The stereo camera pair measures the position of the tracked animal in the sensor frame (subscript *s*) defined to be aligned with one camera. Using measurements of the pan and tilt angles of the camera mount, this position vector is transformed into the vehicle frame (subscript *v*) where control loops are closed using the vehicle's thrusters. The control loops position the vehicle such that the specimen is always in the fields-of-view of both cameras. The control system operates in a cylindrical

coordinate system centered on the animal that matches its objective - to keep the vehicle pointed at the animal and at a constant distance from it. Thus, the measurement is converted to the form of Equation (1), made up of the distance to the specimen ($r$), relative heading to the specimen ($\psi_{rel}$) and relative altitude ($z_{rel}$).

$$ {}^{j}\mathbf{y}_{v} = \begin{bmatrix} r & \psi_{rel} & z_{rel} \end{bmatrix}^{T} \qquad (1) $$

The closed-loop control system strives to regulate this vector to a constant value that places the object at the center of the views of the cameras.

The control loops are closed using the vehicle's hydraulic thrusters. Vehicle thrusters are set up in three pairs, one to actuate fore/aft and (differentially) yaw, one for lateral motion, and one for vertical. Thrusters do not actively control the vehicle's pitch and roll angles, which are instead stabilized by passive buoyancy moments.

With the specimen maintained in view of the upper cameras, the ROV *Ventana*'s high definition science camera (the large lower camera of Figure 1) is free to move without disturbing the control system. Hence, the scientist may freely pan, tilt, shoulder and zoom this camera to capture close-up film and still photographs.

Complete descriptions the system hardware and of the design of the vision and control algorithms are found in [2],[3].

## 3 IMPROVED INITIALIZATION AND SUSTAINABLE TRACKING

Experience in field testing of the tracking system has shown that initialization of the system by the pilot and sustaining tracking for long periods of time can be difficult. This is primarily due to the small volume (with respect to the cameras) in which the target must be maintained. As the system is applied to small specimens, these require closer standoff distances to be adequately visible, resulting in even tighter control error limits on the tracker.

To redesign the system for easier, more robust operation, the constraints imposed on the control system by the sensor must first be explicitly quantified. This section establishes the relationships between control performance constraints, the size and geometry of the common viewing volume of the stereo camera pair defined by the cameras' viewing cones and relative position, the camera rig's position on the vehicle, and the size of the target specimen.

### 3.1 Constraints Imposed on Control Performance by the Vision Sensor

The size of the shared viewable volume of the cameras for a given target and standoff distance imparts constraints on the performance of the control system (or the pilot during initialization) required to maintain the animal within that volume. These constraints, as a function of the camera and specimen parameters, are quantified in this section.

Figure 5 illustrates the geometry defined by the camera parameters and position, and the size of the tracked animal. Each camera may be parameterized by its field-of-view half-angle, $\omega$, and its distance from the center of the vehicle, $L$. (This analysis is simplified by assuming that pan and tilt angles are zero, without loss of generality.) The tracked animal is represented by its diameter, $D$, and its standoff distance from the camera, $r$.

In addition to the boundaries of the field-of-view of the camera, an effective constraint on distance to the target is imposed by the vision algorithms used to track the animal in each image stream. This constraint takes the form of a minimum percent occupancy of the image that a target must occupy to be discerned consistently from marine snow and other image noise. This occupancy, $O$, depends on the camera field-of-view, the distance to the target and the size of the target, as defined in Equation (2). From experience, the lower limit is approximated at 8% of the image dimension, thus set equal to $.08^2$.

$$ O(r, D, \omega) = \left( \frac{D}{2r \sin(\omega)} \right)^{2} ; O_{\min} \triangleq .08^{2} \qquad (2) $$

For a given $O_{min}$, $D$ and $\omega$, this can be rearranged to define $r_{max}$ as

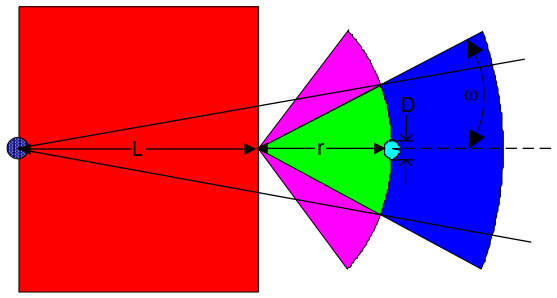


**Figure 5** Parameterization of camera view of target of diameter $D$ with camera with half-angle field-of-view $\omega$. Camera is located $L$ m from the center of the vehicle. View is from above, looking down at vehicle, and camera as illustrated has no pan or tilt angles. Maximum allowable pointing error is given by equation (4).

$$r_{\max}(D,\omega,O_{\min}) = \frac{D}{2\sin(\omega)\sqrt{O_{\min}}} \qquad (3)$$

Thus, $r_{max}$ is the maximum range that the tracker can allow between the camera and the target of diameter $D$ such that it is visible to the vision system using a camera with field-of-view of $2\omega$.

The constraints on pointing and positioning by the controller (or pilot during initialization) may now be defined. For a given set of parameters $r$, $\omega$, $D$, and $L$, the maximum pointing error, $e^{\psi}_{max}$, is given by

$$e^{\psi}_{\max}(r,\omega,D,L) = \tan^{-1}\left(\frac{r\sin(\omega) - D}{L + r}\right) \qquad (4)$$

The maximum error in the camera vertical direction is a function of $r$, the camera's vertical half field-of-view, ${}^{c}\omega^{x}$, and $D$ given by

$${}^{c}e^{x}_{\max}(r, {}^{c}\omega^{x}, D) = r\sin({}^{c}\omega^{x}) - D \qquad (5)$$

The stereo camera pair used in earlier field testing consisted of a narrow field-of-view camera, the Insite Orion and a wide angle camera, the Insite Aurora, aligned vertically (both are products of Insite Pacific, Inc.). When paired with the wide angle Aurora, the entire field-of-view of the Orion is guaranteed to be visible within the view of the wider angle camera. The intersections of the camera fields-of-view are illustrated in Figure 6(a). A photograph of this camera set is included in Figure 7(a).

With this configuration, maximum standoff distance is limited to the smaller distance allowable by the wide angle camera, and the shared viewing volume of the cameras is defined by that standoff distance and the smaller field-of-view of the narrow camera. In both cases, the control performance constraints are limited unfavorably by the worst case camera. The constraints can be calculated by evaluating $e^{\psi}_{max}$ and ${}^{c}e^{x}_{max}$ using Equations (4) and (5) respectively, at $r$ =

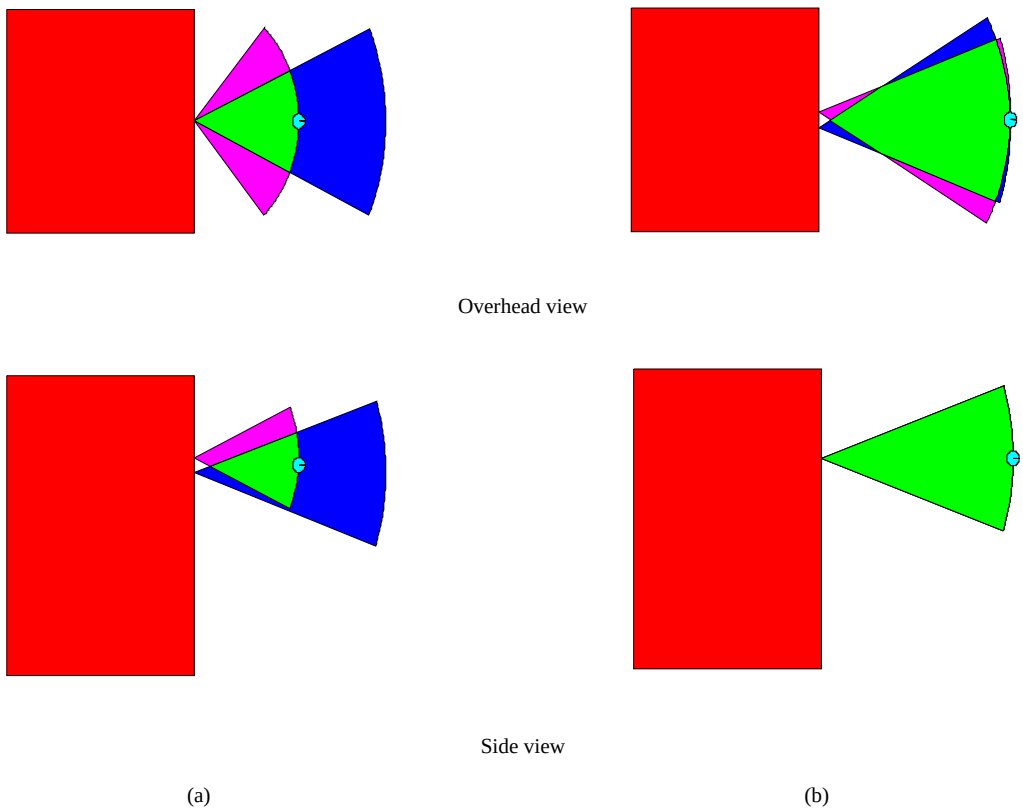


**Figure 6** Stereo vision cone overlap for (a) a wide/narrow camera pair aligned vertically and parallel and (b) a narrow/narrow camera pair horizontally aligned and converging at a 10 degree angle. Both illustrate the maximum range to target based on the worst case $O_{min}$ constraint for the camera set. The stereo vision sensor was redesigned from the configuration of (a) to that of (b) to increase the volume in which the target can be seen.

$r_{max}^{wide}$ and $\omega = \omega_{narrow}$. The results are tabulated in the left hand entries of Table 1 for several diameters of tracking targets.

### 3.2 A Redesigned Stereo Camera System

Based on the preceding analysis, the camera system was redesigned to enlarge the viewable volume formed by the intersection of the vision cones. Three changes were made: changing to two narrow view cameras, converging the cameras inward toward each other, and aligning them horizontally instead of vertically. A photograph of the redesigned stereo camera pair is shown in Figure 7(b).

The choice of two narrow view cameras gives the advantage of being able to maintain a larger standoff distance to the target. This is due to the minimum occupancy condition and its effect on maximum standoff distance, given by Equations (2) and (3), respectively. The worst case field-of-view used in the previous configuration was the horizontal field-of-view of the wide angle camera, which forced the system to operate very near to the specimen, as shown in Figure 6(a). Now, the worst case field-of-view is the horizontal angle of the narrower camera type, significantly increasing the maximum standoff distance, as illustrated in Figure 6(b).

The new configuration also converges the cameras at a small angle (10 degrees). With identical fields-of-view cameras, some portion of the viewing cone of each camera is not visible in the cone of the other. This problem is mitigated by the small convergence angle, which causes the cones to overlap much more, even at close standoff distances.

Because there will always be some part of the view of each camera not visible by the other, the new configuration aligns the cameras horizontally rather than vertically. This takes advantage of the wider field-of-view in the horizontal angle, which when impinged upon by the incomplete overlap, leaves a larger usable volume overall.

To recompute $e^{\psi}_{max}$ for this system, the extrema of the intersected region are calculated based on the diagram shown in Figure 6(b). Equation (4) cannot be used directly for this case. Instead, the positions of the far extrema of the area shared by both vision cones are calculated, along with an angle with respect to the vehicle center. The pointing error constraint is then half of the difference between the angle made up of the rays from the vehicle's center to those points, and the angle subtended by the target with respect to the vehicle's center. Equation (5) for ${}^{c}e^{x}_{max}$ is still valid for this configuration, now with the advantage that $r_{max}$ is calculated using the narrow field-of-view.

The right side entries of each column in Table 1 tabulate the results from the new camera configuration. With the new camera design, allowable control errors and standoff distances are increased for all cases.

| $D$ (cm) | $r_{max}$ (m) | | $e^{\psi}_{max}$ (deg) | | ${}^{c}e^{x}_{max}$ (cm) | |
|---|---|---|---|---|---|---|
| 10 | 0.84 | 1.54 | 4.1 | 6.3 | 38 | 41 |
| 5 | 0.42 | 0.77 | 2.5 | 4.1 | 18 | 21 |
| 2.5 | 0.21 | 0.38 | 1.4 | 2.1 | 7 | 10 |

**Table 1** Calculated maximum standoff distances and control errors for different sizes of observation specimen. For each entry, the left value is calculated based for the old camera configuration, while the right value is for the redesigned camera set.

(a) (b)

**Figure 7** Camera sets for relative position sensing: (a) vertically aligned parallel wide angle and narrow angle cameras, (b) horizontally aligned and converging narrow angle cameras.

## 4 MITIGATING SUSTAINED CLOCKING AROUND THE SPECIMEN

In many field demonstrations of the tracking system, sustained clocking around the specimen at steady-state has occurred. This is due to uncompensated lateral forces, which act in the null space of the control system. These forces likely stem from several sources, such as imperfect alignment of the vehicle's thrusters, non-zero null points on the lateral thrusters, and varying drag properties due to the particular equipment installed on the vehicle.

Any disturbances in the vehicle lateral direction operate in the null space of the cylindrical coordinate control system, which was intended to give the pilot a mechanism to circumnavigate the tracked specimen [2],[3]. The mechanics of this effect are illustrated in Figure 8. In addition to being an unintended nuisance, when fielded on the ROV *Ventana*, this phenomenon can quickly lead to unacceptable tether management issues.

To mitigate this problem, a secondary (and optional) heading control loop was added to the system, illustrated in Figure 9. The loop provides closed-loop compensation for unexpected forces in the null space of the primary tracking loops. This has the effect of placing the vehicle at a fixed position on the

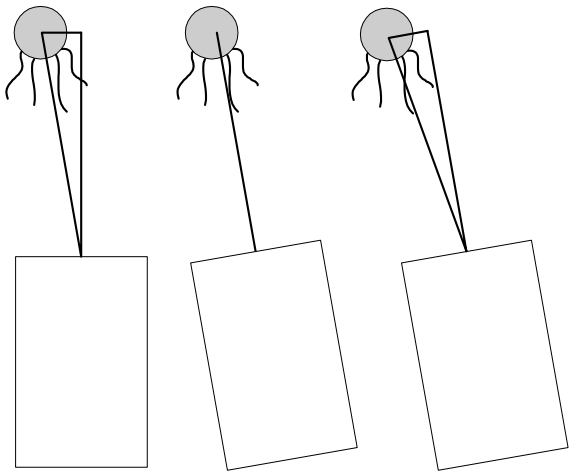

**Figure 8** The effect of yaw/lateral coupling when tracking a midwater specimen, resulting in sustained clocking about the specimen in the null space of the cylindrical coordinate control system. At time step *k* (left), the control system commands a counter-clockwise yaw. The desired result at time step *k+1* is a yaw motion to zero relative heading error (middle). With null space disturbances or uncompensated coupling, the actual result is a combined yaw and lateral motion to starboard, resulting in no net reduction in relative heading error at time step *k+1* (right). As this process continues over time, the vehicle steadily circumnavigates the specimen.

cylindrical coordinate system's circumference (see Figure 3). The ability to circumnavigate the specimen is preserved in this mode by allowing the system's operator to modify the heading reference.

The new heading loop is secondary to the priority control loops that maintain the tracked specimen in view of the control cameras. Therefore it operates separately from the main loops, utilizing the null space inputs in the lateral direction to position the vehicle on the circle. Furthermore, it is designed with a much lower bandwidth than the tracking loops to minimize its effects on the performance of the primary tracking system.

## 5 RECENT RESULTS

### 5.1 Tracking a Wider Variety of Specimens

With the changes in design, a much larger spectrum of animal sizes and types have been tracked by the system, with several examples shown in Figure 4. The example photograph in the lower right of Figure 4, was taken by the tracking system while following an *Aegina* jellyfish. This is a small but mobile jellyfish with diameter on the order of 2 cm, too small to be successfully tracked by the system before modification of the camera system. Detailed tracking data from this demonstration is shown in Figure 10.

Note that the range maintained in this case was less than 0.5 m from the control cameras. The increased viewable volume due to the camera redesign allows operation at this range. With the previous configuration, a specimen of this size would require

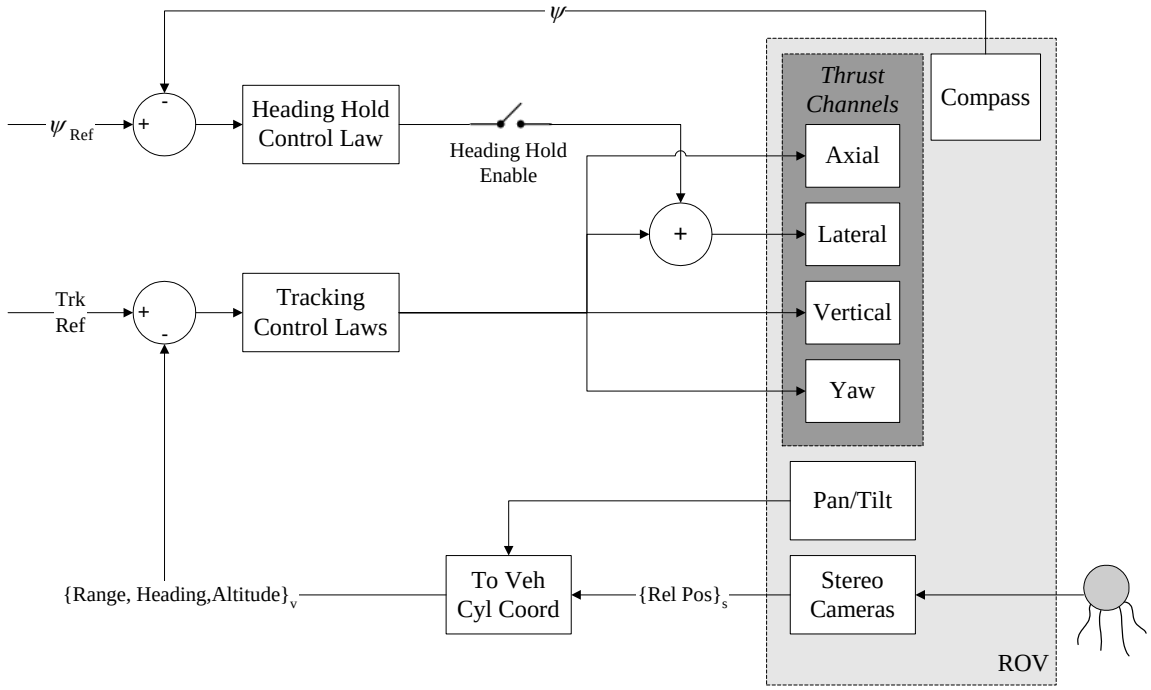


**Figure 9** Control architecture of tracking system, modified to include an optional heading hold loop to stabilize the vehicle's position on the circle about the target.

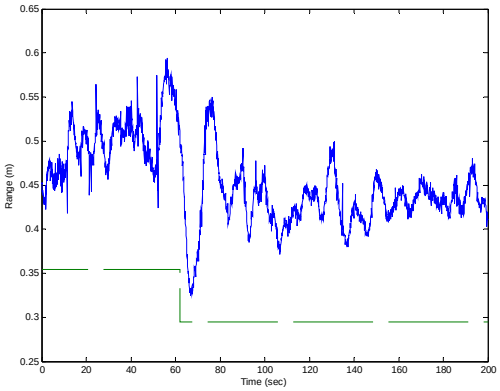


**Figure 10** Range control while tracking an *Aegina* jellyfish. The lower line (dotted) indicates the range reference value. (Offset is due to tether disturbance forces and the lack of an integral control term during this experiment.)

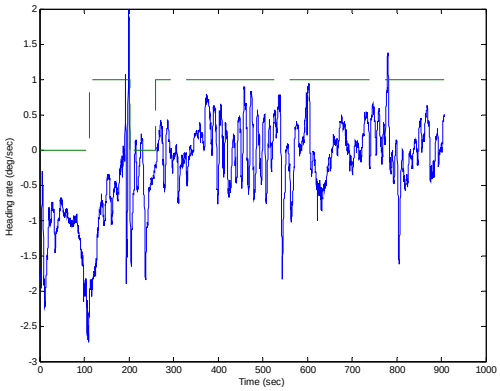


**Figure 11** Demonstration of heading hold performance while tracking a *Solmissus* jellyfish. The solid line is measured yaw rate of the tracking vehicle. The dotted line indicates heading hold on (1) or off (0).

operation at a range of approximately 0.2 m to see it in the wide angle Aurora model camera. Operation at that distance is extremely difficult to initialize by the ROV pilot and difficult for the control system to maintain for a significant length of time.

### 5.2 Heading Hold Control Loop

The heading hold loop has been demonstrated on several tracking demonstrations. An example is shown in Figure 11, where heading hold was toggled on and off while tracking a *Solmissus* jellyfish. This example shows the slow action of the heading hold loop to arrest the clocking motion of the vehicle, which was varying between 1 and 2.5 deg/sec counterclockwise before the heading hold loop was enabled at t = 111 sec.

## 6 CONCLUSION

The partial redesign of the tracking system has improved the operability and effectiveness of the system significantly. By giving the control system a much less constraining volume in which to keep its observation targets, the set of species that is trackable with this system has been expanded to include much smaller and more agile animals. The tracking system now can tolerate larger disturbances without breaking tracking continuity, and the larger operating volume has noticeably improved the ease of initialization by the ROV pilot. With these improvements and the addition of the heading hold loop in the main tracking loops' null space, the system has matured from an experimental prototype to a fully operational pilot aid that is fielded in Monterey Bay, California.

## REFERENCES


1. Rife, J. and Rock, S., "Field Experiments in the Control of a Jellyfish Tracking ROV", *IEEE OCEANS Conference*, Biloxi, MS, 2002, pp. 2031-2038.
2. Rife, J., "Automated Robotic Tracking of Animals in the Deep Ocean", Ph.D. Dissertation, Dept. of Mechanical Engineering, Stanford University, Stanford, CA, 2004.
3. Rife, J. and Rock, S., "Design and Validation of a Robotic Control Law for Observation of Deep-Ocean Jellyfish", *IEEE Transactions on Robotics* (submitted).
4. Robison, B.H. "Deep Pelagic Biology," *Journal of Experimental Marine Biology and Ecology*, 300:253-272, 2004.
5. Robison, B.H. "Midwater Research Methods with MBARI's ROV," *Marine Technology Society Journal*, 26(4):32-39, 1992.
6. Robison, B.H. "The Coevolution of Undersea Vehicles and Deep-Sea Research," *Marine Technology Science Journal*, 33(4):65-73, 1999.
7. Haddock, S.H.D., C.W. Dunn, P.R. Pugh. "A Reexamination of Siphonophore Terminology and Morphology, Applied to the Description of Two New Prayine Species with Remarkable Bio-Optical Properties," *Journal of the Marine Biological Association of the United Kingdom*, 85:695-707, 2005.